PHYSICAL REVIEW B **80**, 094506 (2009)

Origin of the structural phase transition in $BaNi_2As_2$ at 130 K: A combined study of optical spectroscopy and band structure calculations

Z. G. Chen, G. Xu, W. Z. Hu, X. D. Zhang, P. Zheng, G. F. Chen, J. L. Luo, Z. Fang, and N. L. Wang
Beijing National Laboratory for Condensed Matter Physics, Institute of Physics, Chinese Academy of Sciences, Beijing 100190, China

(Received 6 May 2009; revised manuscript received 10 August 2009; published 8 September 2009)

$BaNi_2As_2$ exhibits a first-order structural transition at 130 K. Understanding this structural transition is a crucial step toward understanding the electronic properties of the material. We present a combined optical spectroscopy and band structure calculation study on the compound across the transition. The study reveals that $BaNi_2As_2$ is a good metal with a rather high plasma frequency. The phase transition leads to a small reduction of conducting carriers. We identify that this reduction is caused by the removal of several small Fermi-surface sheets contributed dominantly from the As-As bonding and Ni-As antibonding.

DOI: 10.1103/PhysRevB.80.094506 PACS number(s): 78.40.Kc, 74.25.Gz, 74.25.Jb, 74.70.−b

I. INTRODUCTION

The discoveries of superconductivity in Fe- or Ni-based layered pnictide compounds have generated tremendous interest in condensed-matter community. For the iron arsenic-based compounds not only could they have high superconducting transition temperatures[1–6] but also show intriguing interplay between structure, magnetism, and superconductivity. The undoped compounds commonly display the structural and magnetic phase transitions, which, depending on materials, could occur either at the same temperature or separately.[7–10] Upon electron or hole doping or application of pressure, both the magnetic order and the structural transition are suppressed, and superconductivity emerges.[8,11,12] Intensive studies have been done to elucidate the origin of the structural/magnetic transitions and their relation to superconductivity. The magnetic transitions were identified as itinerant spin-density-wave (SDW) instabilities caused largely by the strong nesting tendency between the hole and electron Fermi surfaces (FS) (Refs. 13 and 14) though conflicting views from a local superexchange picture also exist. The structural phase transition was widely believed to be driven by the magnetic transition.[15,16]

Compared with the FeAs-based compounds, the NiAs-based systems were much less studied. Superconductivity in Ni pnictides has been found in quaternary ZrCuSiAs structure type LaNiPO (T_c=4 K),[2] LaNiAsO (T_c=2.7 K),[17] and $ThCr_2Si_2$ structure type ANi_2As_2 (A=Ba,Sr) (T_c=0.6–0.7 K).[18–20] Although the Ni-pnictide superconductors share the same Ni_2As_2 PbO-type structure as Fe pnictides, the superconducting transition temperatures are much lower, never exceed 5 K even upon doping.[17] Nevertheless, a first-order phase transition at T_s=130 K, much similar to the AFe_2As_2 (A=Ca,Sr,Ba), is found for $BaNi_2As_2$ compound.[18,20] Initially, by analogy with FeAs-based 122 compounds, the transition was considered as a magnetic SDW transition concomitant with the a structural transition.[18] However, to date no evidence for magnetic transition was reported. Much remain unknown about this transition. It is highly interesting to study the origin of the first-order phase transition and compare with their FeAs analogies.

In this work we report the optical spectroscopy study on $BaNi_2As_2$ single crystals. The study reveals remarkable differences between $BaNi_2As_2$ and $BaFe_2As_2$. In accord with the presence of two more electrons in 3d orbitals, the $BaNi_2As_2$ shows a much higher plasma frequency (or carrier density). By lowering the temperature across the transition, part of the spectral weight from conducting electrons is removed and shifted to high energies. However, unlike the case of $BaFe_2As_2$, where an SDW gap opens at low frequencies,[21] the spectral weight redistribution for $BaNi_2As_2$ occurs over a much broader energy scale. The study reveals that the first-order phase transition in $BaNi_2As_2$ is essentially different from the SDW-type phase transition as observed in $BaFe_2As_2$, thus against the presence of competing phase such as magnetic SDW order in Ni pnictides. To understand the spectral change across the transition, we performed first-principles calculations of the band structure. We illustrate that the transition is mainly caused by the removal of several small Fermi-surface sheets with dominant As-As $pp\sigma$ bonding and Ni-As $dp\sigma*$ antibonding characters. Other orbitals/bands are less affected and remain conductive.

II. EXPERIMENTS AND RESULTS

Single crystals of $BaNi_2As_2$ were grown using Pb-flux method similar to the procedure described by Ronning *et al.*,[18] except that we use a much slower cooling rate of 3.5 °C from 1100 °C to 650 °C. The Pb fluxes were removed by using a centrifuge at 650 °C. Resistivity measurement, as shown in the inset of Fig. 1, indicates metallic behavior with a small resistivity value of about 50 $\mu\Omega$ cm at 300 K. The resistivity shows a jump at 130 K on cooling, then becomes more metallic at low temperature, similar to the case of $CaFe_2As_2$. Finally, $BaNi_2As_2$ enters into superconducting state at 0.65 K. All those are in good agreement with previous reports in literature.[18,20]

The optical-reflectance measurements were performed on a combination of Bruker IFS 66v/s and 113v on newly cleaved surfaces (ab plane) of those crystals up to 25 000 cm^{-1}. An *in situ* gold and aluminum overcoating technique was used to get the reflectivity R(ω). The real part of conductivity $\sigma_1(\omega)$ is obtained by the Kramers-Kronig transformation of R(ω).

Figure 1 shows the experimental reflectance spectra up to 25 000 cm^{-1}. A rather good metallic response is observed.

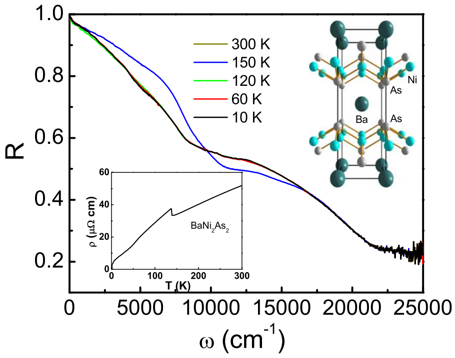

FIG. 1. (Color online) Reflectance curves up to 25 000 cm^{-1} (~3 eV) at different temperatures. Upper inset shows the crystal structure. Lower inset shows the T-dependent dc resistivity.

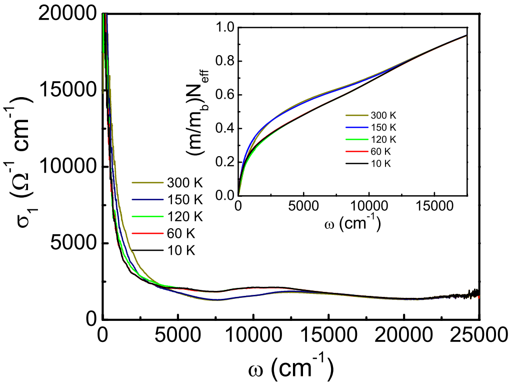

FIG. 2. (Color online) Optical conductivity spectra over broad frequencies. Inset shows the effective carrier density per Ni site estimated from the spectral weight under conductivity curves.

R(ω) approaches to unity at zero frequency and shows a plasma edgelike shape near 10 000 cm^{-1}. Note that this edge frequency is substantially higher than that in BaFe$_2$As$_2$, which is seen around only 3000 cm^{-1} where it merges into the relatively high values of mid-infrared reflectance contributed mainly by the interband transitions.[21] This gives direct evidence that the conducting carrier density in BaNi$_2$As$_2$ is much higher than that in BaFe$_2$As$_2$. A quantitative estimation of the plasma frequency will be given below. There is only a minor change in R(ω) as temperature decreases from 300 to 150 K. However, by cooling across the phase transition at 130 K, R(ω) shows a dramatic change. Except for the reflectance at very low frequency, R(ω) is suppressed significantly below the reflectance edge, but enhanced in the frequency range of 9 000–16 000 cm^{-1}. With further decreasing temperature, the spectral change becomes very small. The very low frequency R(ω) increases slightly, reflecting enhanced metallic dc conductivity. In the mean time, a weak suppression in the mid-infrared region near 5000 cm^{-1} could be resolved.

The above mentioned spectral change in R(ω) across the transition is very different from BaFe$_2$As$_2$ which shows an SDW order concomitant with the structural transition at 140 K. For BaFe$_2$As$_2$, the most prominent spectral change is a substantial suppression in R(ω) at low frequencies, roughly below 1000 cm^{-1}, which is ascribed to the opening of an SDW gap in the magnetic ordered state.[21] For BaNi$_2$As$_2$, the spectral change occurs over a much broader frequency range. Besides the weak suppression feature near 5000 cm^{-1}, there is no additional spectral suppression at lower energies.

Figure 2 shows the conductivity spectra $\sigma_1(\omega)$ up to 25 000 cm^{-1}. The Drude-type conductivity can be observed for all spectra at low frequencies. When temperature drops below 130 K, part of the spectral weight is transferred from below 7000 cm^{-1} to higher energies. The effective carrier density per Ni site below a certain energy ω can be obtained by the partial sum rule

$$\frac{m}{m_b}N_{eff}(\omega) = \frac{2mV_{cell}}{\pi e^2 N}\int_0^{\omega}\sigma_1(\omega')d\omega', \tag{1}$$

where m is the free-electron mass, m$_b$ is the averaged high-frequency optical or band mass, V_{cell} is a unit-cell volume, N the number of Ni ions per unit volume. The inset of Fig. 2 shows $(m/m_b)N_{eff}$ as a function of frequency for different temperatures. We find that the spectral weight is recovered roughly near 12 000 cm^{-1}. N_{eff} is related to an overall plasma frequency, after choosing a proper high-frequency limit ω_c, via the relationship $\omega_p^2=4\pi e^2 N_{eff}(\omega_c)/m_b(V_{cell}/N)=8\int_0^{\omega_c}\sigma_1(\omega')d\omega'$. Choosing $\omega_c \approx 7500$ cm^{-1}, a frequency where $\sigma_1(\omega)$ reaches its minimum but below the interband transition, we get the overall plasma frequency $\omega_p \approx 3.49\times10^4$ cm^{-1} for $T=300$ K and 150 K. If we choose the same cutoff frequency at 7500 cm^{-1}, we get $\omega_p \approx 3.33\times10^4$ cm^{-1} for $T=10$, 60, and 120 K. However, it should be noted that the conductivity spectra already show a weak peak feature near 5000 cm^{-1}, this results in an overestimate of the plasma frequency at low temperatures. Note that the plasma frequency for BaFe$_2$As$_2$ is only around 1.3×10^4 cm^{-1} in the nonmagnetic phase,[21] so BaNi$_2$As$_2$ has a much higher plasma frequency. This is in accord with the presence of two more electrons in 3d orbitals.

An alternative way of making quantitative analysis is to fit the conductivity spectra by a Drude-Lorentz model to isolate the different components of the electronic excitations.[21] The Drude component represents the contribution from conduction electrons while the Lorentz components describe the interband transitions. Usually a single Drude term is used to extract the conduction-electron contribution but here we found that two Drude components could reproduce the low-frequency conductivity much better. This could be naturally accounted for by the multiple band characteristic of the material. Similar two Drude component analysis has been applied to the optical data of EuFe$_2$As$_2$,[22] pointing toward a generic behavior for those multiple band systems. The general formula for the Drude-Lorentz model is

$$\sigma_1(\omega) = \sum \frac{\omega_{pi}^2}{4\pi}\frac{\Gamma_{Di}}{\omega^2+\Gamma_{Di}^2} + \sum \frac{S_j^2}{4\pi}\frac{\Gamma_j\omega^2}{(\omega_j^2-\omega^2)^2+\omega^2\Gamma_j^2}, \tag{2}$$

where ω_{pi} and Γ_{Di} are the plasma frequency and the relaxation rate of each conduction band while ω_j, Γ_j, and S_j are the resonance frequency, the damping, and the mode strength of each Lorentz oscillator, respectively. It is found that the conductivity curve above the phase transition could be well

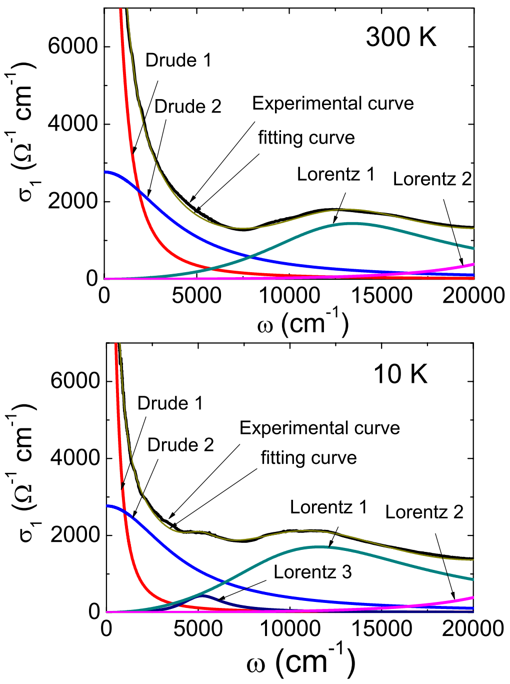

FIG. 3. (Color online) Optical conductivity spectra at 300 and 10 K together with the fitting curves from the Drude-Lorentz model.

reproduced by two Drude components and two Lorentz oscillators. Below the transition temperature, an additional Lorentz oscillator is required to fit the curve. Figure 3 shows the spectra and fitting curves at two representative temperatures 300 and 10 K. The parameters for the two Drude components are summarized in Table I for different temperatures. The overall plasma frequency is obtained as $\omega_p = \sqrt{\omega_{p1}^2 + \omega_{p2}^2}$. We find that the values are roughly in agreement with those obtained by the sum-rule analysis.

We can now summarize our main findings from the optical data. $BaNi_2As_2$ has a much higher plasma frequency than $BaFe_2As_2$. By lowering the temperature across the transition, part of the spectral weight from conducting electrons was removed and shifted to higher energies. There is a small peak near 5000 cm^{-1} but its spectral weight could not compensate for the loss of the low-frequency Drude component, the spectral weight loss is recovered at a much higher energy scale. The spectral change across the transition is very different from the situation of $BaFe_2As_2$ for which an SDW gap opens at low frequencies, roughly below 1000 cm^{-1}.[21]

TABLE I. The fitting parameters of two Drude components in Eq. (2) at different temperatures. The unit for ω_{pi} and Γ_{Di} is cm^{-1}.

T (K)	ω_{p1}	Γ_{D1}	ω_{p2}	Γ_{D2}	ω_p
10	2.10×10^4	410	2.59×10^4	4050	3.33×10^4
60	2.10×10^4	410	2.59×10^4	4050	3.33×10^4
120	2.19×10^4	490	2.59×10^4	4050	3.39×10^4
150	2.50×10^4	510	2.59×10^4	4050	3.59×10^4
300	2.74×10^4	730	2.59×10^4	4050	3.77×10^4

III. STRUCTURAL DISTORTION AND BAND STRUCTURE CALCULATIONS

The key issue here is the origin of the first-order phase transition in $BaNi_2As_2$. As mentioned above, a magnetic SDW transition concomitant with a structural transition was initially suggested only by analogy with FeAs-based 122 compounds. However, to date no evidence for magnetic transition was reported. Furthermore, the band structure calculations reveal that the Fermi surfaces of $BaNi_2As_2$ are markedly different from that of FeAs-based 122 compounds, the Fermi surface becomes much larger in $BaNi_2As_2$,[23,24] and no nesting of the Fermi surfaces could be identified. One would not expect that the phase transitions in these two systems have the same origin. Very recently, the crystal structure after the transition was determined. It is found that $BaNi_2As_2$ experiences a structural phase transition from a high-T tetragonal phase to a low-T triclinic phase. Examining carefully the bondings between atoms, we find that the As-As distance along the c axis increases from 3.553 Å to 3.584 Å, while within ab plane, the Ni ions change from a square lattice to zigzag chains where short Ni-Ni bonds (~2.8 Å) are separated by longer Ni-Ni distances (~3.1 Å).[20]

For the $ThCr_2Si_2$-type transition-metal-based compounds AM_2X_2, three different types of bondings, M-X, M-M, and X-X, and their contributions to different bands in the electronic structure were well studied.[25,26] It is known that two dispersive bands which cross the E_F lightly and have mainly the X-X bonding (X-X $pp\sigma$) and M-X antibonding (M-X $dp\sigma*$) character are rather sensitive to the positions of X ions and show strong electron-phonon coupling effect.[26] To see the effect of the lattice distortion on the band structure, we performed local density-approximation band structure calculations for $BaNi_2As_2$ using the experimentally determined crystal structures[20] below and above the phase transition as an initial input and then relax the atom positions. We find that the change in the optimized structure from the experimentally determined one is rather small, less than 2% in both atom positions and lattice parameters. A lowering of energy of 6 meV/unit cell is obtained for the distorted structure. The calculated results are presented in Fig. 4. Here, a standard notation of the Brillouin zone for a simple tetragonal lattice is used for illustrating the band dispersions. For comparison reason, we also map the Brillouin zone for the low-T triclinic lattice to the original tetragonal phase. A minor shift in the high-symmetry line is due to the lattice-parameter difference. We find that most of the dispersive bands keep unchanged except for some small shifts in energy but the band dispersions close to Fermi level near Z' point and along R'-X' direction are dramatically altered. Those bands are dominantly contributed from the As-As $pp\sigma$ bonding and Ni-As $dp\sigma*$ antibonding states. In the high-T symmetry phase, those bands cross the E_F and lead to a very flat electron type FS surrounding Z' point and eight three-dimensional (3D) hole type FSs along R-X line [see Fig. 4(b)]. However, in the low-T phase, the FS near Z' point tends to vanish completely, leading to a gap roughly about 0.5 eV. Additionally, the hole-type 3D FSs along R'-X' line are completely gone due to the band splitting [Fig. 4(c)]. This splitting has a smaller energy scale 0.2–0.3 eV. This

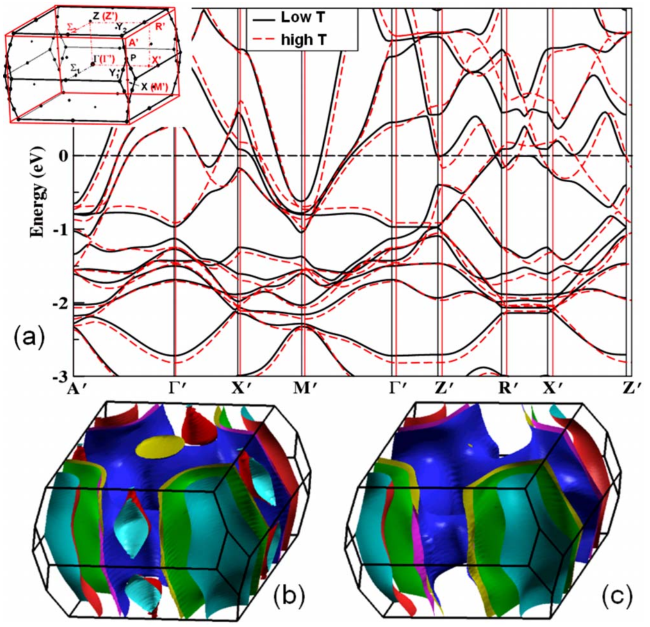

FIG. 4. (Color online) (a) The band structures for $BaNi_2As_2$ both above (red dash) and below (black) the phase transition. [(b) and (c)]: the Fermi surfaces in the high-T and low-T phases, respectively.

could give the onset of the small mid-infrared peak shown in lower panel of Fig. 3. Compared with the rather big FS sheets by other bands, the areas enclosed by those FSs are rather small, so the reduction in the carrier density below the transition is small, which is also in agreement with the optical measurement results.

We can see that the driving mechanism for the structural phase transition is still electronic. The energy gain through gapping the small FS sheets is not due to the nesting effect of FS but mainly caused by the removal/instability of several specific bands near E_F whose energy levels are particularly sensitive to the direct As-As and Ni-As bondings.

IV. CONCLUSIONS

We have performed a combined optical spectroscopy and first principles calculation study on a Ni-pnictide compound $BaNi_2As_2$ in an effort to understand the origin of the structural phase transition at 130 K. Our study reveals that the electronic properties and the structural phase transition of $BaNi_2As_2$ are essentially different from those of Fe pnictides AFe_2As_2 (A=Ba, Sr, Ca). $BaNi_2As_2$ is a good metal with a much higher plasma frequency. The phase transition leads to a small reduction in conducting carriers. Remarkably, there is no SDW-type gap opening at low frequency as observed for AFe_2As_2 (A=Ba, Sr, Ca). The study indicates that the structural phase transition is not driven by the nesting of Fermi surfaces. Instead, it is more likely caused by a reduction in the single-electron energy contributed dominantly from the bands with As-As bonding and Ni-As antibonding characters which are coupled strongly with the lattice. The small reduction in the conducting carriers is ascribed to the removal of several small Fermi-surface sheets in the distorted structure.

ACKNOWLEDGMENTS

This work is supported by the National Science Foundation of China, the Chinese Academy of Sciences, and the 973 project of the Ministry of Science and Technology of China.

---

[1] Y. Kamihara, H. Hiramatsu, M. Hirano, R. Kawamura, H. Yanagi, T. Kamiya, and H. Hosono, J. Am. Chem. Soc. **128**, 10012 (2006).

[2] T. Watanabe, H. Yanagi, T. Kamiya, Y. Kamihara, H. Hiramatsu, M. Hirano, and H. Hosono, Inorg. Chem. **46**, 7719 (2007).

[3] Y. Kamihara, T. Watanabe, M. Hirano, and H. Hosono, J. Am. Chem. Soc. **130**, 3296 (2008).

[4] X. H. Chen, T. Wu, G. Wu, R. H. Liu, H. Chen, and D. F. Fang, Nature (London) **453**, 761 (2008).

[5] G. F. Chen, Z. Li, D. Wu, G. Li, W. Z. Hu, J. Dong, P. Zheng, J. L. Luo, and N. L. Wang, Phys. Rev. Lett. **100**, 247002 (2008).

[6] Z. A. Ren, J. Yang, W. Lu, W. Yi, X. L. Shen, Z. C. Li, G. C. Che, X. L. Dong, L. L. Sun, F. Zhou, and Z. X. Zhao, Europhys. Lett. **82**, 57002 (2008).

[7] C. de la Cruz, Q. Huang, J. W. Lynn, J. Li, W. R. Ii, J. L. Zarestky, H. A. Mook, G. F. Chen, J. L. Luo, N. L. Wang, and P. Dai, Nature (London) **453**, 899 (2008).

[8] M. Rotter, M. Tegel, and D. Johrendt, Phys. Rev. Lett. **101**, 107006 (2008).

[9] J. H. Chu, J. G. Analytis, C. Kucharczyk, and I. R. Fisher, Phys. Rev. B **79**, 014506 (2009).

[10] G. F. Chen, W. Z. Hu, J. L. Luo, and N. L. Wang, Phys. Rev. Lett. **102**, 227004 (2009).

[11] Jun Zhao, Q. Huang, Clarina de la Cruz, Shiliang Li, J. W. Lynn, Y. Chen, M. A. Green, G. F. Chen, G. Li, Z. Li, J. L. Luo, N. L. Wang, Pengcheng Dai, Nature Mater. **7**, 953 (2008).

[12] M. S. Torikachvili, S. L. Bud'ko, N. Ni, and P. C. Canfield, Phys. Rev. Lett. **101**, 057006 (2008).

[13] J. Dong, H. J. Zhang, G. Xu, Z. Li, G. Li, W. Z. Hu, D. Wu, G. F. Chen, X. Dai, J. L. Luo, Z. Fang, and N. L. Wang, Europhys. Lett. **83**, 27006 (2008).

[14] D. J. Singh, Physica C **469**, 418 (2009).

[15] T. Yildirim, Phys. Rev. Lett. **101**, 057010 (2008).

[16] C. Fang, H. Yao, W.-F. Tsai, J. P. Hu, and S. A. Kivelson, Phys. Rev. B **77**, 224509 (2008); C. Xu, M. Muller, and S. Sachdev, *ibid.* **78**, 020501(R) (2008).

[17] Z. Li, G. F. Chen, J. Dong, G. Li, W. Z. Hu, D. Wu, S. K. Su, P. Zheng, T. Xiang, N. L. Wang, J. L. Luo, Phys. Rev. B **78**, 060504(R) (2008).

[18] F. Ronning, N. Kurita, E. D. Bauer, B. L. Scott, T. Park, T. Klimczuk, R. Movshovich, and J. D. Thompson, J. Phys.: Condens. Matter **20**, 342203 (2008).

[19] E. D. Bauer, F. Ronning, B. L. Scott, and J. D. Thompson, Phys. Rev. B **78**, 172504 (2008).

[20] A. S. Sefat, M. A. McGuire, R. Jin, B. C. Sales, D. Mandrus, F. Ronning, E. D. Bauer, and Y. Mozharivskyj, Phys. Rev. B **79**,

094508 (2009).

[21] W. Z. Hu, J. Dong, G. Li, Z. Li, P. Zheng, G. F. Chen, J. L. Luo, and N. L. Wang, Phys. Rev. Lett. **101**, 257005 (2008).

[22] D. Wu, N. Barisic, N. Drichko, S. Kaiser, A. Faridian, M. Dressel, S. Jiang, Z. Ren, L. J. Li, G. H. Cao, Z. A. Xu, H. S. Jeevan, and P. Gegenwart, Phys. Rev. B **79**, 155103 (2009).

[23] A. Subedi and D. J. Singh, Phys. Rev. B **78**, 132511 (2008).

[24] I. R. Shein and A. L. Ivanovskii, Phys. Rev. B **79**, 054510 (2009).

[25] R. Hoffmann and C. Zheng, J. Phys. Chem. **89**, 4175 (1985).

[26] D. Johrendt, C. Felser, O. Jepsen, O. K. Andersen, A. Mewis, and J. Rouxel, J. Solid State Chem. **130**, 254 (1997).